Progress In Electromagnetics Research M, Vol. 64, 109–121, 2018

Investigation of the Effects of Different Magnetization Patterns on the Performance of Series Hybrid Excitation Synchronous Machines

Alireza Hoseinpour*, Mohamed Mardaneh, and Akbar Rahideh

Abstract—In this paper, the effects of magnetization patterns on the performance of series hybrid excitation synchronous machines (SHESMs) are investigated. SHESMs have three magnetic field sources: armature winding currents, permanent magnets and auxiliary winding current. To initiate the investigation, the magnetic field distributions produced by these three sources are obtained. Using the magnetic field distributions, the machine is analyzed under no-load and on-load conditions. Furthermore, the operational indices, such as inductance, torque, and unbalance magnetic force, are calculated. Various magnetization patterns are considered to investigate their influences on the performance of the machine.

1. INTRODUCTION

The permanent magnet synchronous machines (PMSMs) are widely used in industry due to their high efficiency and torque to volume ratio [1]. In spite of their advantages, their flux control capabilities are limited due to the constant permanent magnet flux [2], including in surface mounted PMSMs. In order to overcome this weakness, it is recommended to use PMSMs with an auxiliary excitation. These machines are named hybrid excitation synchronous machines (HESMs).

HESMs are divided into two types: series HESMs (SHESMs) and parallel HESMs (PHESMs) [3–6]. In SHESMs, the permanent magnet flux and auxiliary winding (AW) flux pass through the same path, which leads to less iron losses [3]. The machines can operate in the flux-enhancing mode when the fluxes are in the same directions, and if the fluxes are in the opposite directions, the machine is in the flux-weakening mode of operation. In SHESMs, there is higher probability of demagnetization because the whole AW flux passes through the permanent magnets, and the flux controllability is reduced due to low permanent magnet permeability [3, 5, 6]. In PHESMs, the risk of demagnetization is reduced, and controllability is increased. However, the iron losses are increased because the flux routes of excitation sources are different [3, 6].

If both field sources are placed in the stator, not only there is no need for retaining sleeve, but also the heat is removed more easily (it is assumed that the machine has an internal rotor). However, the mutual torque is not generated, and the end winding effects are considerable [7]. Some of structures of the machine [8, 9] limit the available space for the winding, so the diameter of the stator should be high. Therefore, the torque to volume ratio decreases [10].

If the magnet is on the rotor and AW in the stator, the reluctance and mutual torque are produced. However, retaining sleeve is required, and iron losses increase. In order to reduce iron losses, an external rotor structure can be used [11]. This structure needs retaining sleeve.

If both of the field excitation sources are located on the rotor, mutual and reluctance torque components are generated. This machine can be employed in constant power applications [10] with

Received 20 October 2017, Accepted 23 January 2018, Scheduled 5 February 2018
* Corresponding author: Alireza Hoseinpour (a.hoseinpour@uoz.ac.ir).
The authors are with the Shiraz University of Technology, Iran.

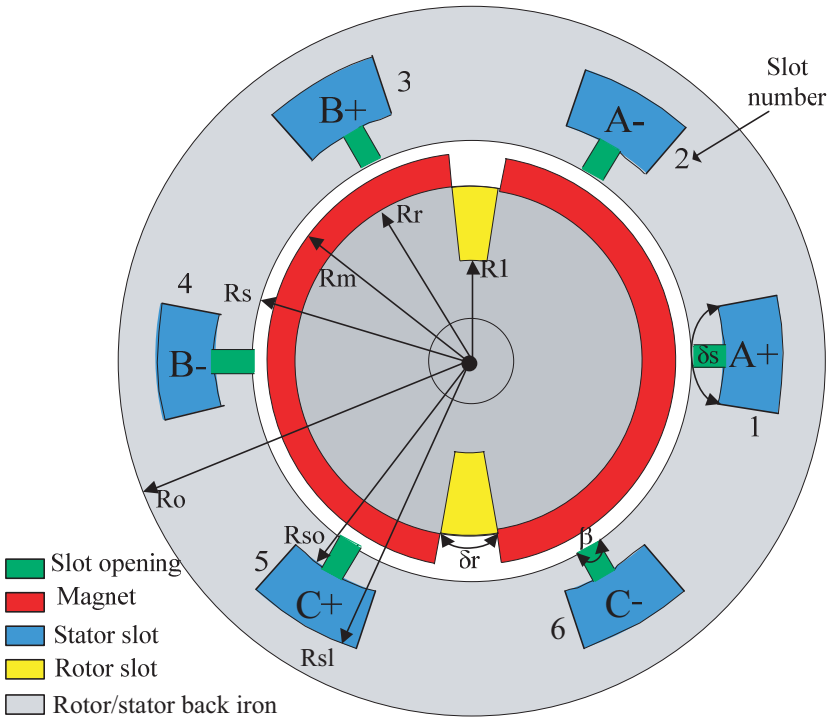

Figure 1. Configuration of SHESM.

speed variations. However, the existence of brushes and retaining sleeve is the disadvantage of this structure [9].

Therefore, a SHESM in which both excitation sources are on the rotor is selected. Three structures are suggested, and both of the excitations are located on the rotor: spoke [12], buried [13] and surface mounted (SM) [14]. Among these three types, the SM, which is one of the SHESMs, is chosen. The structure of a SHESM is shown in Figure 1.

Various types of magnetization patterns are reported for PMSMs [15] in which the radial magnetization (RM), parallel magnetization (PM) and Halbach magnetization (HM) are more popular. The type of magnetization pattern highly influences the magnetic flux density distribution. Therefore, the performance of the machine is significantly affected by the magnetization pattern. HSEM has been analyzed with PM pattern and open circuit condition in [14]. In the present paper, three types of magnetization (RM, PM, and HM) are considered, and the SHESM is analyzed for open-circuit and on-load modes of operation

In addition, two different layouts for the stator winding exist. The first one is non-overlapping, and the second one is overlapping. Moreover, non-overlapping type is divided into alternate-teeth wound and all-teeth wound [16]. It is assumed that the armature winding is alternate-teeth wound for the SHESM.

In this paper, first the method of calculating the magnetic field is explained for a magnetostatic analysis. Then, the torque, unbalance magnetic force (UMF), and inductance are determined for a rotating SHESM. After that, to evaluate the effects of the magnetization pattern on the machine performances three types of magnetization are simulated, and their results are compared.

2. ANALYSIS OF SHESM

2.1. Calculation of Magnetic Flux Density

The governing partial differential equation in the presence of magnetization and external current is as follows:

$$\nabla^2 \mathbf{A} = -\mu_0 \mu_r \mathbf{J} - \mu_0 \nabla \times \mathbf{M} \tag{1}$$

where μ_0, μ_r, $\mathbf{J}$, $\mathbf{A}$ and $\mathbf{M}$ are permeability of free space, relative permeability of magnet, current density, vector magnetic potential and remanent magnetization vector, respectively. In regions where there is current but no magnetization (e.g., winding regions), the following relation can be expressed.

$$\nabla^2\mathbf{A} = -\mu_0\mu_r\mathbf{J} \tag{2}$$

In regions where there is magnetization but no current (e.g., permanent magnet regions), the following expression is applied.

$$\nabla^2\mathbf{A} = -\mu_0\nabla\times\mathbf{M} \tag{3}$$

In regions where there is neither current nor magnetization (e.g., ai-gap region), the Laplace equation can be written.

$$\nabla^2\mathbf{A} = 0 \tag{4}$$

These equations are solved, and the magnetic flux density components are calculated using

$$\mathbf{B}= \nabla\times\mathbf{A}$$

.

2.2. Energy Calculation

The magnetic energy of a system is given by the following expressions. The expressions represent total values of energy for the volumes taken into account. Note that the integrals have simpler expressions if the material property of the domain has linear characteristics. In the case of linear characteristics, the magnetic energy and co-energy values are identical ($w = w_c$).

$$w = w_c = \int_V \left(\int_0^{\mathbf{B}} \mathbf{H}\cdot d\mathbf{B}\right) dV \tag{5}$$

where V is the volume of the machine.

2.3. UMF Calculation

The radial and tangential forces are calculated by Maxwell stress tensor. First, the flux density should be computed, then the mentioned magnetic pull is obtained by the following relations.

$$f_r = \frac{1}{2\mu_0}\left(B_r^2 - B_\theta^2\right) \tag{6}$$

$$f_\theta = \frac{1}{\mu_0}B_rB_\theta \tag{7}$$

where B_r and B_θ are the radial and tangential components of the flux density vector, respectively. Besides, f_r and f_θ are the radial and tangential components of the magnetic pull, respectively. These equations can be transformed into the Cartesian system.

$$f_x = f_r\cos(\theta) - f_\theta\sin(\theta) \tag{8}$$

$$f_y = f_r\sin(\theta) + f_\theta\cos(\theta) \tag{9}$$

where f_x and f_y are the components of the magnetic pull in x and y directions, respectively. Then, UMF is determined with the integration of Eqs. (8) and (9) in the middle of the air gap.

$$F_x = \int_{-L/2}^{L/2}\int_{-\pi}^{\pi} f_x r d\theta dz = L\int_{-\pi}^{\pi} f_x r d\theta \tag{10}$$

$$F_y = \int_{-L/2}^{L/2}\int_{-\pi}^{\pi} f_y r d\theta dz = L\int_{-\pi}^{\pi} f_y r d\theta \tag{11}$$

$$|F| = \sqrt{F_x^2 + F_y^2} \tag{12}$$

where F_x, F_y and $|F|$ are the x-component, y-component and amplitude of the UMF, respectively, and L is the motor axial length.

2.4. Torque Calculation

The instantaneous torque ($\mathbf{T_{inst}}$) is computed by $\mathbf{T} = \mathbf{r} \times \mathbf{F}$ as follows

$$\mathbf{r} = r\mathbf{a_r}$$

$$\mathbf{F} = F_r\mathbf{a_r} + F_\theta\mathbf{a}_\theta = \iint (f_r\mathbf{a_r} + f_\theta\mathbf{a}_\theta)\, dldz$$

$$\mathbf{T_{inst}} = \mathbf{r} \times \mathbf{F} = (r\mathbf{a_r}) \times \iint (f_r\mathbf{a_r} + f_\theta\mathbf{a}_\theta)\, dldz \overset{dl=rd\theta}{\Longrightarrow} \frac{1}{\mu_0} \int_{-\frac{L}{2}}^{\frac{L}{2}} \int_{-\pi}^{\pi} r^2 B_r B_\theta d\theta dz \mathbf{a_z} \tag{13}$$

$$\mathbf{T_{inst}} = \frac{L}{\mu_0} r^2 \int_{-\pi}^{\pi} B_r B_\theta d\theta \mathbf{a_z}$$

where $\mathbf{a_r}$, $\mathbf{a}_\theta$ and $\mathbf{a_z}$ are the cylindrical axes unit vectors, and $\mathbf{r}$ is the distance vector between the applied force and the axis of rotation.

The instantaneous torque has three components. The first one is the cogging torque; the second one is the reluctance torque; the last one is the mutual torque. In order to compute the cogging torque, the permanent magnet and AW are active, and stator armature winding is open-circuited. In contrast, just the armature winding should be excited to calculate the reluctance torque. The mutual torque is achieved by the interaction between the field excitations and the armature excitation.

2.5. Inductance Calculation

The self-inductance of each phase and the mutual-inductance between two phases are computed by the following equations

$$w_{ii} = \frac{1}{2} L_{ii} I_i^2 \rightarrow L_{ii} = \frac{2w_{ii}}{I_i^2} \tag{14a}$$

$$w_{ij} = L_{ij} I_i I_j \rightarrow L_{ij} = \frac{w_{ij}}{I_i I_j} \tag{14b}$$

where I_i and I_j are the currents of phases i and j, respectively; w_{ii} is the stored energy when only phase i is carrying current; w_{ij} is the total energy when both phases i and j are carrying current minus w_{ii} and w_{jj}.

2.6. Magnetization

Among different permanent magnet materials, in this investigation, Nd-FeB is employed. This material has a linear B-H curve in the second quadrant. Due to the presence of rotor slots, only radial-, parallel- and Halbach magnetization patterns can be used [15]. These magnetizations are depicted in Figure 2.

The radial and tangential components of the radial magnetization are presented in Eqs. (15) and (16), respectively.

$$M_r = \begin{cases} \dfrac{B_{rem}}{\mu_0} & |\theta| \leq \dfrac{\pi}{2p}\alpha_p \\ 0 & \dfrac{\pi}{2p}\alpha_p \leq |\theta| \leq \dfrac{\pi}{2p}(2-\alpha_p) \\ -\dfrac{B_{rem}}{\mu_0} & \dfrac{\pi}{2p}(2-\alpha_p) \leq |\theta| \leq \dfrac{\pi}{p} \end{cases} \tag{15}$$

$$M_\theta = 0 \tag{16}$$

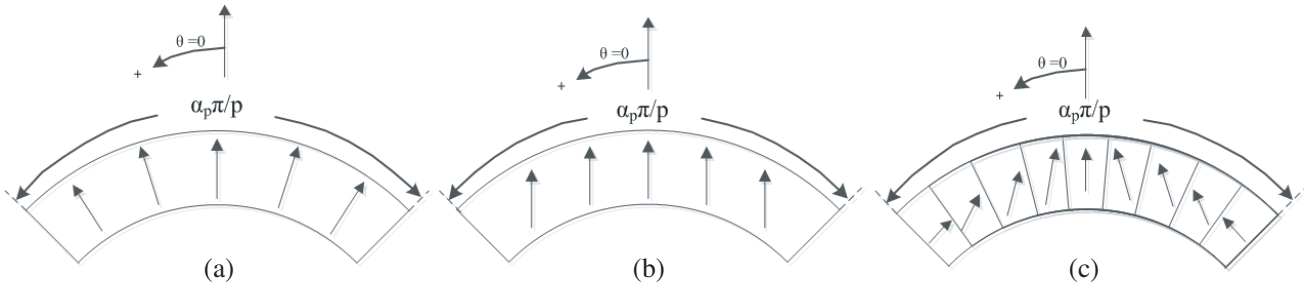

Figure 2. Magnetization patterns: (a) radial magnetization; (b) parallel magnetization; (c) Halbach magnetization.

These components are described for PM as below

$$M_r = \begin{cases} \dfrac{B_{rem}}{\mu_0}\cos(p\theta) & |\theta| \le \dfrac{\pi}{2p}\alpha_p \\ 0 & \dfrac{\pi}{2p}\alpha_p \le |\theta| \le \dfrac{\pi}{2p}(2-\alpha_p) \\ -\dfrac{B_{rem}}{\mu_0}\cos\left(p\theta\left(1-\dfrac{\pi}{|\theta|\,p}\right)\right) & \dfrac{\pi}{2p}(2-\alpha_p) \le |\theta| \le \dfrac{\pi}{p} \end{cases} \tag{17}$$

$$M_\theta = \begin{cases} -\dfrac{B_{rem}}{\mu_0}\sin(p\theta) & |\theta| \le \dfrac{\pi}{2p}\alpha_p \\ 0 & \dfrac{\pi}{2p}\alpha_p \le |\theta| \le \dfrac{\pi}{2p}(2-\alpha_p) \\ \dfrac{B_{rem}}{\mu_0}\sin\left(p\theta\left(1-\dfrac{\pi}{|\theta|\,p}\right)\right) & \dfrac{\pi}{2p}(2-\alpha_p) \le |\theta| \le \dfrac{\pi}{p} \end{cases} \tag{18}$$

Finally, radial and tangential components for HM are presented as follows.

$$M_r = \begin{cases} \dfrac{B_{rem}}{\mu_0}\left[\cos(p\theta) - \cos\left(\dfrac{\pi p\alpha_p}{2}\right)\right] & |\theta| \le \dfrac{\pi}{2p}\alpha_p \\ 0 & \dfrac{\pi}{2p}\alpha_p \le |\theta| \le \dfrac{\pi}{2p}(2-\alpha_p) \\ \dfrac{B_{rem}}{\mu_0}\left[\cos(p\theta) + \cos\left(\dfrac{\pi p\alpha_p}{2}\right)\right] & \dfrac{\pi}{2p}(2-\alpha_p) \le |\theta| \le \dfrac{\pi}{p} \end{cases} \tag{19}$$

$$M_\theta = \begin{cases} 0 & \dfrac{\pi}{2p}\alpha_p \le |\theta| \le \dfrac{\pi}{2p}(2-\alpha_p) \\ -\dfrac{B_{rem}}{\mu_0}\sin(p\theta) & \text{otherwise} \end{cases} \tag{20}$$

3. SIMULATION RESULTS

According to Figure 1, the center of the permanent magnet is aligned with the first slot of the stator, and the layout of the stator winding is alternate-teeth wound. The specifications of the machine are presented in Table 1, and three types of magnetization patterns are considered. Since the presented model is 2-D, the end effect is ignored. Normally the end effects are negligible if the machine axial length is larger than the machine diameter. Initially the magnetic flux density components are computed by magnetostatic analysis. After that, the machine rotor moves in the dynamic analysis, and the torque, the self and mutual inductances of the stator windings and UMF are calculated.

Table 1. Parameters of the SHESM.

Parameters	symbols	Values
Stator-slot span angle	δ_s	0.6283 rad
Stator-slot-opening span angle	β	0.4398 rad
Rotor-slot span angle	δ_r	0.4712 rad
Outer radius of machine	R_o	105 mm
Outer radius of the stator-slots	R_{sl}	81.5 mm
Outer radius of the stator-slot-opening	R_{so}	62.9 mm
Stator bore radius	R_s	57.5 mm
Magnet Radius	R_m	56 mm
Rotor back-iron radius	R_r	50 mm
Inner rotor-slot radius	R_1	26.5 mm
Pole arc to pole pitch ratio	α_p	0.85
Remanence flux density of PM	B_{rem}	1 T
Relative recoil permeability of PM	μ_r	1.05
Cross sectional area of wire in stator and rotor	A_c	1.2 mm^2
Rotor DC current	I_r	10 A
Stator peak current	I_m	14.14 A
Per-phase number of stator winding turns	N_{ts}	422
Number of rotor winding turns per pole-pair	N_{tr}	212
The rms of input phase voltage	V^i_{rms}	492 V
Motor axial length	L	90 mm

3.1. Magnetostatic Analysis

According to the principle of superposition, the impact of each resource is individually assessed, thus this analysis is divided into three stages. The permanent magnet, AW, and stator winding are separately considered in the mentioned order.

First, it is assumed that the PMs are active, and both AW and stator coils are open-circuited. The radial and tangential components of the magnetic flux density vector due to permanent magnets with three types of magnetization in the middle of air-gap are shown in Figure 3.

After evaluating the effects of permanent magnets, the AW effects are investigated. The trend of the generated magnetic flux density due to AW, as shown in Figure 4, is similar to that of the RM permanent magnet; however, the magnitude of the magnetic flux density due to AW is lower than that of the permanent magnet Therefore, permanent magnet and AW are the main and auxiliary field sources, respectively.

The effect of three-phase stator windings is known as the armature reaction. The three-phase sinusoidal currents are shown in Figure 5. As evident from Figure 5 at initial time, the phases a, b, and c have, respectively, zero, negative, and positive values. The radial and tangential components of the magnetic flux density due to armature current are shown in Figures 6(a) and (b), respectively.

3.2. Dynamic Analysis

In contrast to the magnetostatic analysis in which the simulation is carried out at a specific time and at specific rotor angular position, the dynamic analysis is carried out during a period of time at which the rotor is rotated at a proper rotational velocity. Therefore, the x-axis of the dynamic results is the rotor angular position with respect to the rotor initial position. In the following, the inductance, torque, and

UMF are calculated for the case study.

The mutual inductance between stator winding phases is independent of the type of magnetization, and it depends on the configuration of the stator winding and machine dimensions. The individual flux linkage of each phase is more than the coupling flux with other phases, thus the self-inductance value is more than that of the mutual inductance. Since the angle between phases is 120 degrees, the mutual inductance value is negative. Furthermore, as shown in Figure 7, both self and mutual inductances of the stator windings vary with rotor position because of the salient structure of the rotor.

The instantaneous torque has three components: reluctance, cogging, and mutual components. In this SHESM, the reluctance torque is produced by armature excitation, thus it is independent of the magnetization. The reluctance torque is shown in Figure 8(a). In contrast to the reluctance torque, the cogging and mutual torques are affected by the magnetization type. Therefore, the instantaneous torque is also affected by the magnetization pattern of PM. As evident from Figure 8(b), HM develops lower amount of the cogging torque compared to the other two magnetization patterns. Therefore in

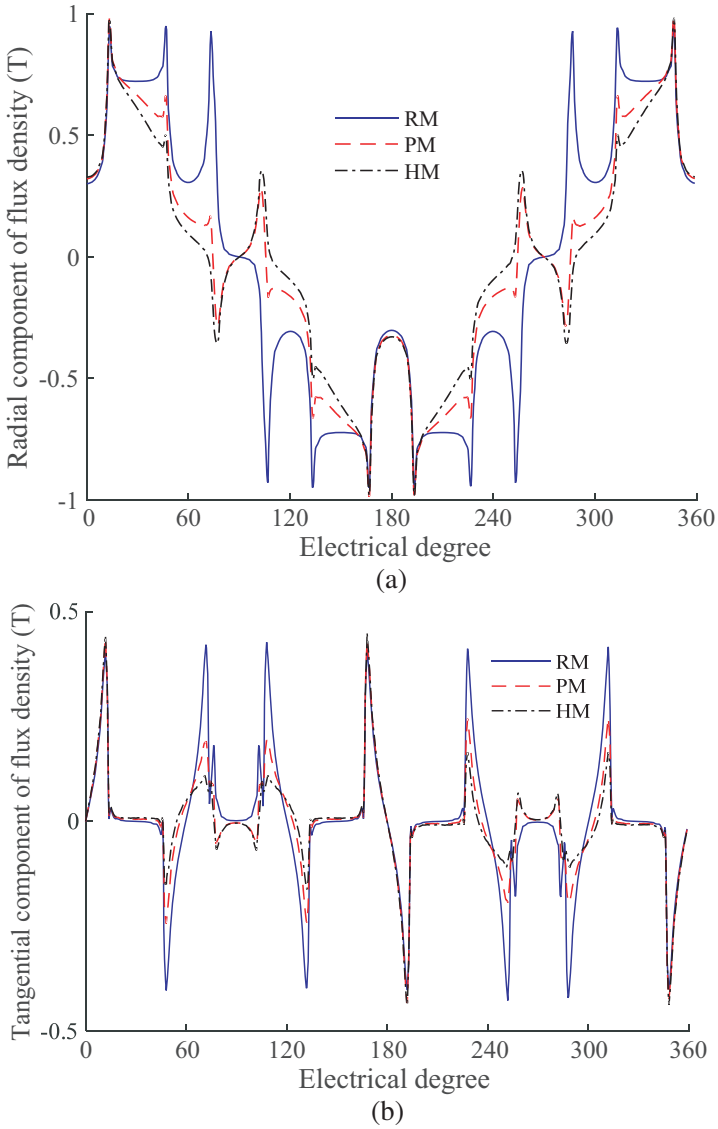

Figure 3. Magnetic flux density components due to permanent magnets for various magnetization patterns: (a) radial component; (b) tangential component.

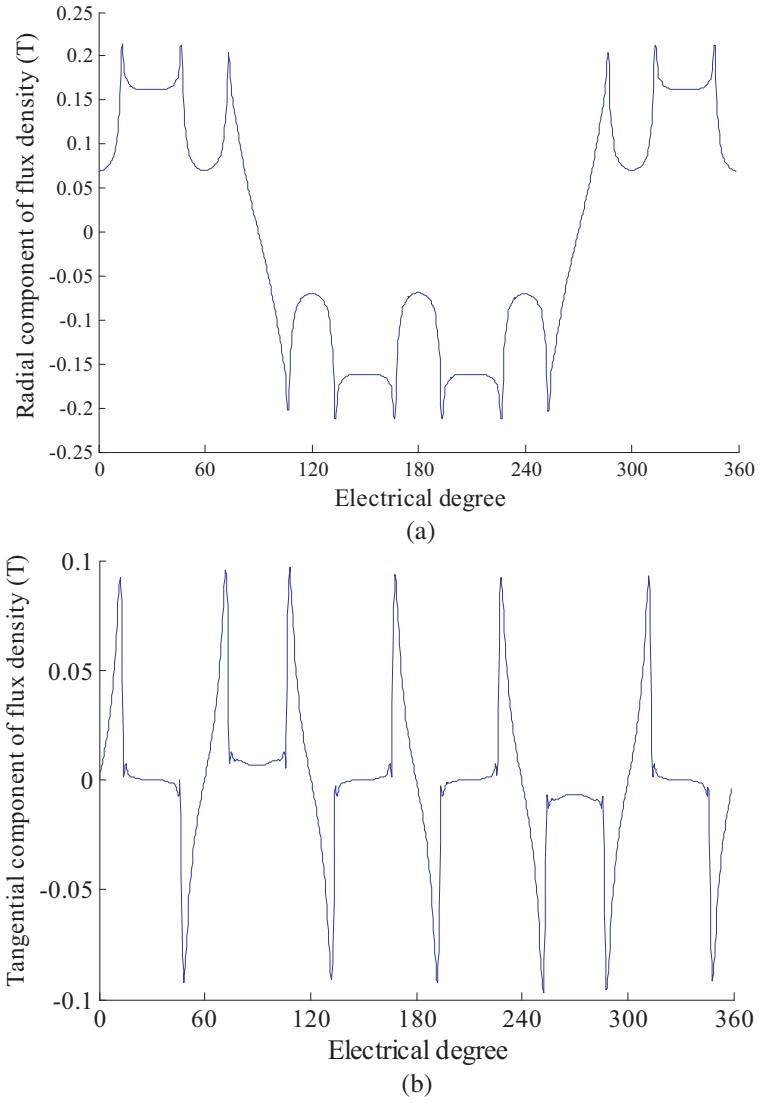

Figure 4. Magnetic flux density due to auxiliary winding: (a) radial component; (b) tangential component.

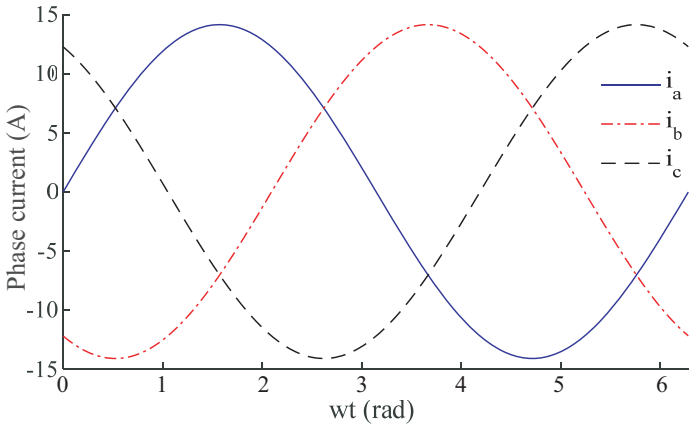

Figure 5. Three-phase armature currents.

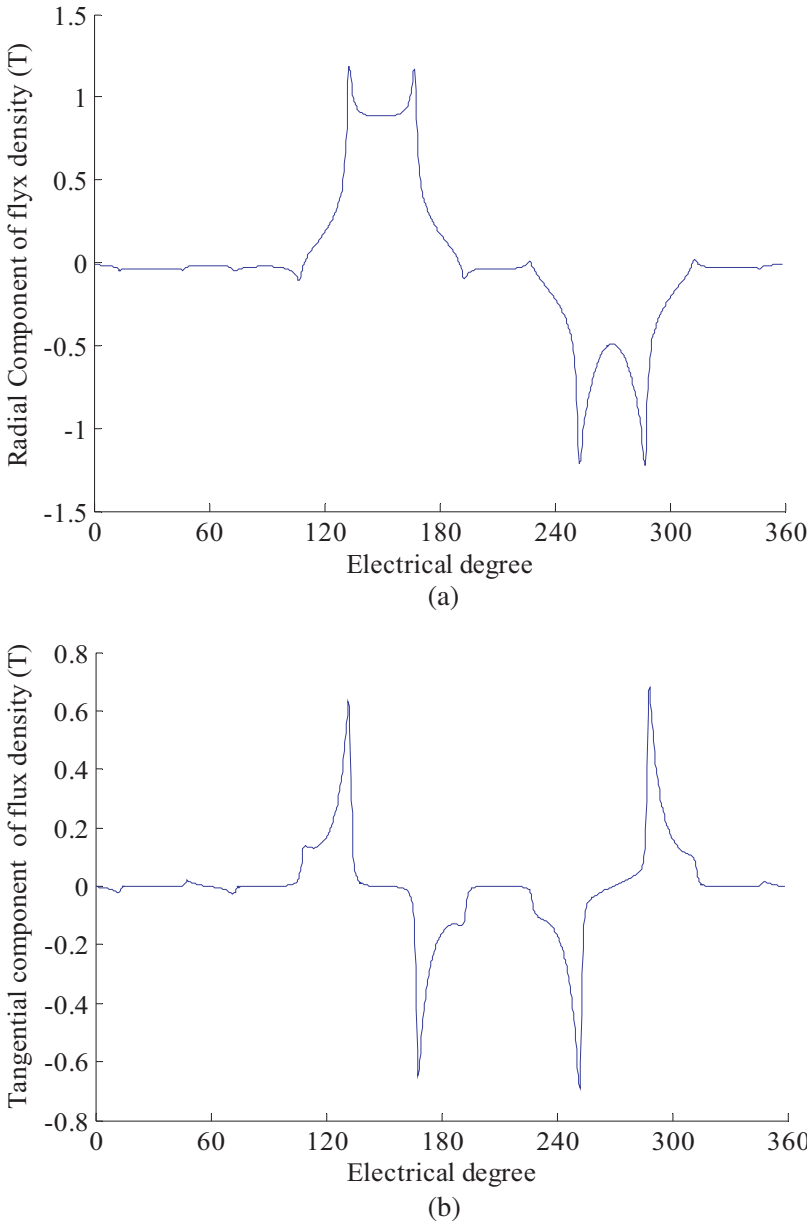

Figure 6. Magnetic flux density components due to armature currents: (a) radial component; (b) tangential component.

terms of cogging torque, HM outperforms the other two magnetization patterns.

The average amounts of the instantaneous torque for RM, PM, and HM are 34.68, 29.88, and 27.37 N.m., respectively. Therefore, the machine equipped with the radial magnetization pattern produces higher average torque; however, it is not recommended for applications where low torque ripple is of prime importance. The unbalanced magnetic forces can be divided into two components along the x and y-axes. The two components for the machines with three magnetization patterns are shown in Figures 9(a) and 9(b). The magnitude of the force is shown in Figure 9(c). It can be deduced from Figure 9 that the HM produces less UMF.

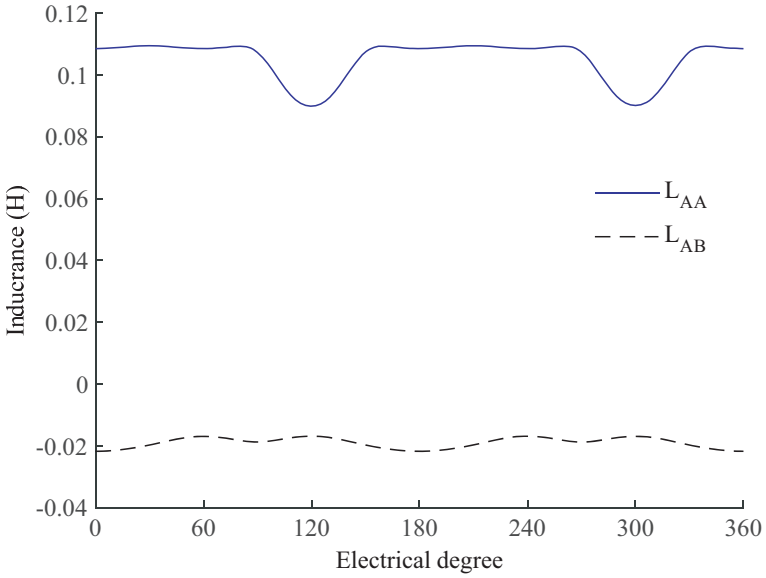

Figure 7. Self and mutual inductances of the stator winding.

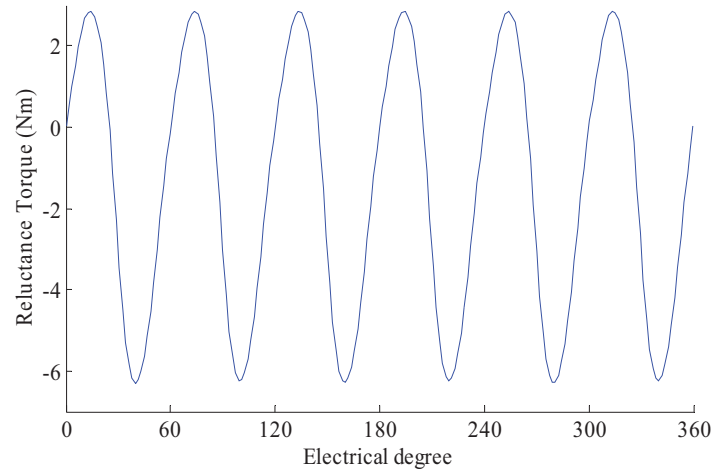

(a)

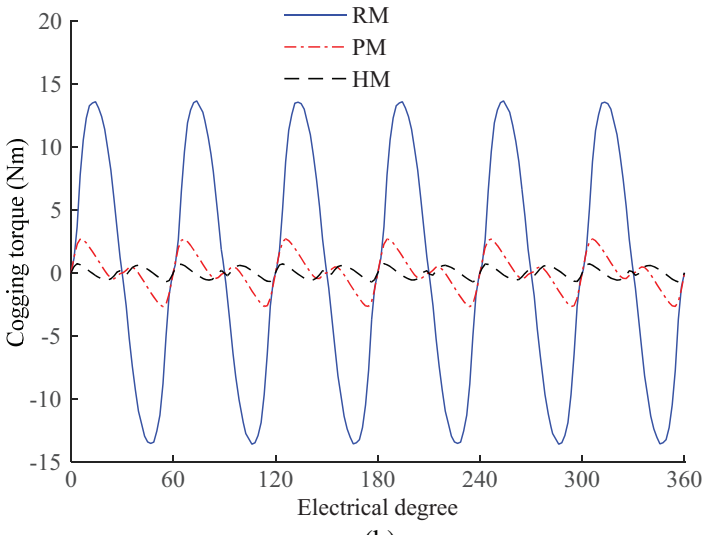

(b)

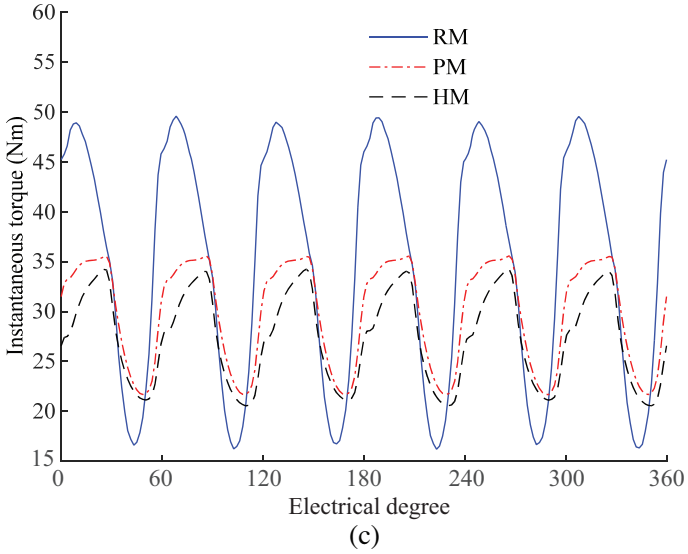

Figure 8. (a) Reluctance torque; (b) Cogging torque due to three magnetization patterns; (c) Instantaneous torque for RM, PM, and HM.

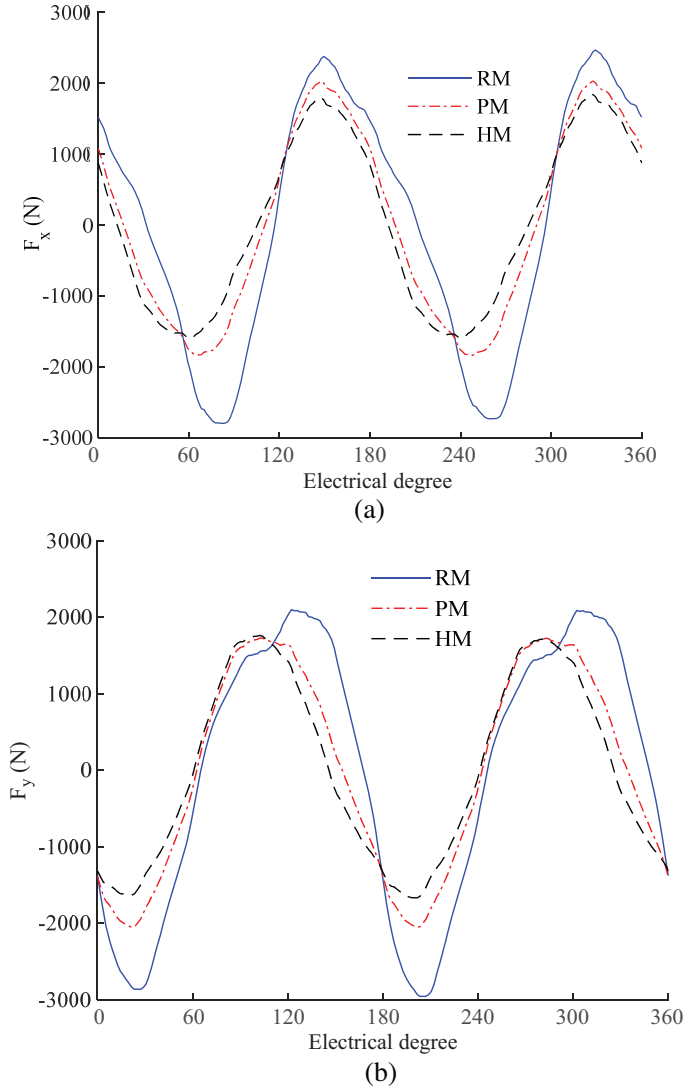

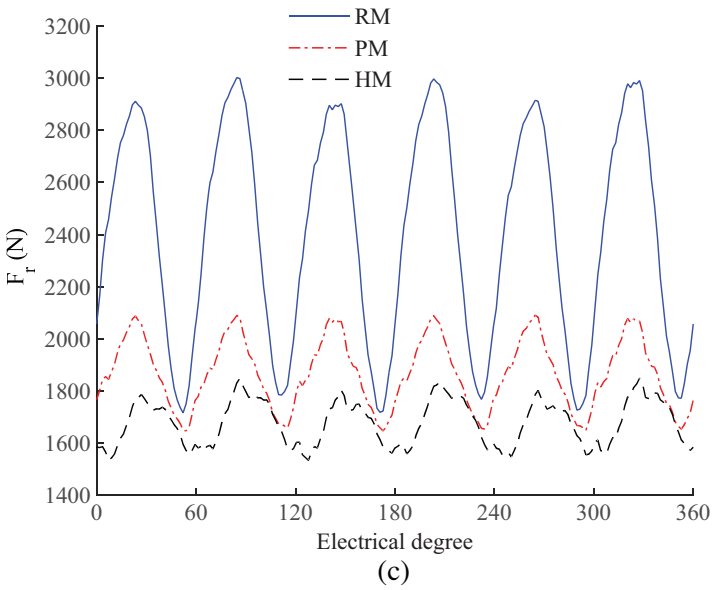

Figure 9. (a) UMF in x direction; (b) UMF in y direction; (c) The magnitude of UMF.

4. CONCLUSION

In this paper, a SHESM has been analyzed, and the effects of different magnetization patterns have been investigated on its performance. High average instantaneous torque is achieved with the radial magnetization pattern while low cogging torque, torque ripple and UMF are obtained with the Halbach magnetization pattern.

REFERENCES

1. Knypñski, Ł., L. Nowak, and A. Demenko, "Optimization of the synchronous motor with hybrid permanent magnet excitation system," *The International Journal for Computation and Mathematics in Electrical and Electronic Engineering*, Vol. 34, No. 2, 448–455, 2015.
2. Amara, Y., J. Lucidarme, M. Gabsi, M. Lécrivain, A. H. Ben Ahmed, and A. D. Akémakou, "A new topology of hybrid excitation synchronous machine," *IEEE Transactions on Industrial Application*, Vol. 37, No. 5, 1273–1281, Sep./Oct. 2001.
3. Amara, Y., S. Hlioui, R. Belfkira, G. Barakat, and M. Gabsi, "Comparison of open circuit flux control capability of a series double excitation machine and a parallel double excitation machine," *IEEE Transactions on Vehicular Technology*, Vol. 60, No. 9, Nov. 2011.
4. Wang, Y. and Z. Deng, "Hybrid excitation topologies and control strategies of stator permanent magnet machines for DC power system," *IEEE Transactions on Industrial Electronics*, Vol. 59, No. 12, 2012.
5. Geng, W., Z. Zhang, K. Jiang, and Y. Yan, "A new parallel hybrid excitation machine: Permanent-magnet/variable-reluctance machine with bidirectional field-regulating capability," *IEEE Transactions on Industrial Electronics*, Vol. 62, No. 3, Mar. 2015.
6. Kamiev, K., J. Pyrhönen, J. Nerg, V. Zaboin, and J. Tapia, "Modeling and testing of an armature-reaction-compensated (PM) synchronous generator," *IEEE Transactions on Energy Conversion*, Vol. 28, No. 4, Dec. 2013.
7. Zhu, X., M. Cheng, W. Hua, J. Zhang, and W. Zhao, "Design and analysis of a new hybrid excited doubly salient machine capable of field control," *Conference. Rec. IEEE IAS Annu. Meeting*, Vol. 5, 2382–2389, Tampa, FL, USA, 2006.

8. Hua, W., M. Cheng, and G. Zhang, "A novel hybrid excitation flux switching motor for hybrid vehicles," *IEEE Transactions on Magnetics*, Vol. 45, No. 10, 4728–4731, Oct. 2009.
9. Owen, R. L., Z. Q. Zhu, and G. W. Jewell, "Hybrid-excited flux-switching permanent-magnet machines with iron flux bridges," *IEEE Transactions on Magnetics*, Vol. 46, No. 6, 1726–1729, Jun. 2010.
10. Zhang, Z., S. Ma, J. Dai, and Y. Yan, "Investigation of hybrid excitation synchronous machines with axial auxiliary airgaps and nonuniform airgaps," *IEEE Transactions on Industrial Application*, Vol. 50, No. 3, May/Jun. 2014.
11. Luo, X. and T. A. Lipo, "A synchronous/permanent magnet hybrid AC machine," *IEEE Transactions on Energy Conversion*, Vol. 15, No. 2, 203–210, Jun. 2000.
12. Kim, S. I., J. Cho, S. Park, T. Park, and S. Lim, "Characteristics comparison of a conventional and modified spoke-type ferrite magnet motor for traction drives of low-speed electric vehicles," *IEEE Transactions on Industrial Application*, Vol. 49, No. 6, 2516–2523, 2013.
13. Kamiev, K., J. Nerg, J. Pyrhönen, V. Zaboin, and J. Tapia, "Feasibility of an armature-reaction-compensated permanent-magnet synchronous generator in island operation," *IEEE Transactions on Industrial Electronic*, Vol. 61, No. 9, Sep. 2014.
14. Bali, H., Y. Amara, G. Barakat, R. Ibtiouen, and M. Gabsi, "Analytical modeling of open circuit magnetic field in wound field and series double excitation synchronous machines," *IEEE Transactions on Magnetics*, Vol. 46, No. 10, Oct. 2010.
15. Rahideh, A., M. Mardaneh, and T. Korakianitis, "Analytical 2-D calculations of torque, inductance, and Back-EMF for brushless slotless machines with surface inset magnets," *IEEE Transactions on Magnetics*, Vol. 49, No. 8, 1–12, Aug. 2013.
16. Teymoori, S., A. Rahideh, H. Moayed-Jahromi, and M. Mardaneh, "2-D analytical magnetic field prediction for consequent-pole permanent magnet synchronous machines," *IEEE Transactions on Magnetics*, Vol. 52, No. 6, 1–14, Jun. 2016.